Available online at www.sciencedirect.com
ScienceDirect
Journal of Power Sources 171 (2007) 894–903
JOURNAL OF POWER SOURCES
www.elsevier.com/locate/jpowsour

Structural and electrochemical properties of $LiNi_{1/3}Co_{1/3}Mn_{1/3}O_2$: Calcination temperature dependence

Yasuhiro Fujii [a,b,*], Hiroshi Miura [a], Naoto Suzuki [a], Takayuki Shoji [a], Noriaki Nakayama [b,1]

[a] *Tosoh Co., Ltd., 4560 Kaisei-cho, Syunan, Yamaguchi 746-8501, Japan*
[b] *Graduate School of Science and Technology, Yamaguchi University, 2-16-1 Tokiwadai, Ube 755-8611, Japan*

Received 5 January 2007; received in revised form 12 June 2007; accepted 12 June 2007
Available online 19 June 2007

Abstract

The structure of the layered $LiNi_{1/3}Co_{1/3}Mn_{1/3}O_2$ has been investigated by powder X-ray diffraction and electron diffraction, and the relationship of the calcination temperature with the crystal structure, morphology and electrochemical properties has been studied. All the unit cell parameters increase monotonically with increasing the calcination temperature. Some of the [00.1] zone electron diffraction patterns for the sample calcined at higher temperature than 1000 °C show extra spots indicating the 2×2 ordering in the basal triangular lattice. These results indicate that the high temperature calcination leads to the formation of vacancies in the transition metal layers with the spinel-like ordering. The calcination at higher temperature lowers the specific capacities and degrades the cycle performances, while the packing density of the powder is increased by the sintering. The optimum calcination temperature is 900 °C in order to obtain the electrochemically active and dense packed oxide particles. The decrease of Li composition leads to coprecipitation of the spinel-like second phase in the range of $0.742 \leq x \leq 0.884$ for $Li_xNi_{1/3}Co_{1/3}Mn_{1/3}O_2$, when calcined at 900 °C. The Li-deficient samples show the worse electrochemical properties similarly to the stoichiometric samples calcined at high temperature. For the Li-excess samples, no impurity phase has been detected and their cycle performances are improved.

Keywords: Lithium batteries; Cathode materials; Electron diffraction

1. Introduction

The rechargeable Li-ion batteries in widespread use as power sources for electronic devices are based on the reversible storage of Li atoms in the crystal lattice of the anode and cathode materials. In recent years, Li–Ni–Co–Mn–O compounds with layered rock-salt type structures have been proposed as possible alternatives to $LiCoO_2$ widely used in current Li-ion batteries. Above all, $LiNi_{1/3}Co_{1/3}Mn_{1/3}O_2$ is one of the most possible candidates with good electrochemical performances, safety, low toxicity and low cost [1–4]. This material shows the rechargeable capacity of about 200 mAh g^{-1} in the voltage range from 2.5 to 4.6 V. The thermal behavior of the fully charged state for $LiNi_{1/3}Co_{1/3}Mn_{1/3}O_2$ with electrolyte is much better than that of $LiCoO_2$ or $LiNiO_2$.

One inconvenient feature of this compound is the low tap density of samples prepared by typical laboratory syntheses. The low packing density of powders in the electrode leads to the low volumetric capacity in the practical Li-ion batteries [5]. Densely packed oxides powders can be obtained from Ni–Co–Mn mixed hydroxides using a well controlled co-precipitation method [6]. The sintering of the particles by high temperature calcinations also increases the packing density of powders in the electrode. However, the phase stability of $LiNi_{1/3}Co_{1/3}Mn_{1/3}O_2$ as a function of the calcination temperature has not been well investigated.

The principal aim of the present study is to clarify the structural details of the $LiNi_{1/3}Co_{1/3}Mn_{1/3}O_2$ calcined at high temperatures and their correlation to the electrochemical properties. Another aim is to optimize the calcination temperature for electrochemically active and densely packed electrodes. We have synthesized $LiNi_{1/3}Co_{1/3}Mn_{1/3}O_2$ samples at different

* Corresponding author at: Tosoh Co., Ltd., 4560 Kaisei-cho, Syunan, Yamaguchi 746-8501, Japan. Tel.: +81 834 63 9914; fax: +81 834 63 9896.
E-mail addresses: ya_fujii@tosoh.co.jp (Y. Fujii), nakayamn@yamaguchi-u.ac.jp (N. Nakayama).
[1] Fax: +81 836 85 9601.

0378-7753/$ – see front matter © 2007 Elsevier B.V. All rights reserved.
doi:10.1016/j.jpowsour.2007.06.017

temperatures in the range from 800 to 1150 °C. The Ni–Co–Mn mixed hydroxides powders were used as the precursor with the proper size distribution and the low specific surface area suitable for practical electrodes. We also investigated the effect of Li content on the crystal structure of $Li_xNi_{1/3}Co_{1/3}Mn_{1/3}O_2$ ($0.742 \leq x \leq 1.12$) calcined at 900 °C.

2. Experimental

$LiNi_{1/3}Co_{1/3}Mn_{1/3}O_2$ was prepared by heating the appropriate mixtures of lithium hydroxide and Ni–Co–Mn mixed hydroxide at different temperatures from 800 to 1150 °C for 12 h in air stream. Excess Li was added to compensate for the Li loss by volatilization. The amount of excess Li were increased with raising the calcination temperature to obtain the nearly stoichiometric samples. Samples with the nominal compositions, $Li_xNi_{1/3}Co_{1/3}Mn_{1/3}O_2$ ($x = 0.742$, 0.884, 0.999, 1.08, and 1.12) have been also synthesized at 900 °C for 12 h in air stream. The heating and cooling rate of 100 °C h^{-1} was applied for all temperature settings.

The Ni–Co–Mn mixed hydroxide was prepared by a coprecipitation method; the solutions of $NiCl_2$, $CoCl_2$, $MnCl_2$, NaOH and NH_4OH with the appropriate proportion were mixed simultaneously [6]. The synthetic parameters such as pH, the temperature, and so on were controlled by to obtain dense and spherical particles. As shown in a SEM image of Fig. 1, the diameter of particles distributes in the range from 10 to 25 μm with two peaks in the size distribution curve, and the BET specific surface area is 4.0 m^2 g^{-1}.

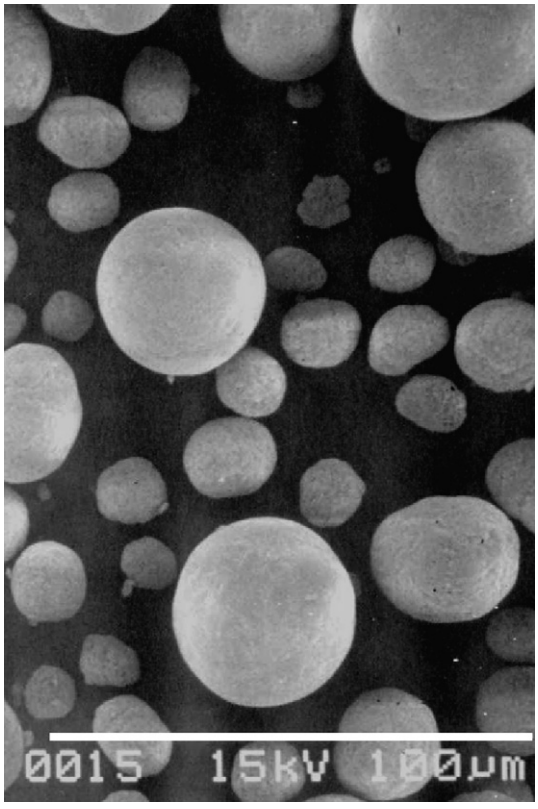

Fig. 1. A SEM image of the Ni–Co–Mn mixed hydroxide particles as a precursor.

Samples were identified and characterized by powder XRD with Cu-Kα radiation and electron diffraction. Rietveld refinements were performed using Rietan-2000 program [7]. For TEM observations, samples were dispersed in ethanol by applying the ultrasonic wave and were collected on a holly micro-grid supported on a copper grid mesh. A field emission type TEM (JEOL JEM2010F) operated at 200 kV was used for the observations. Chemical compositions and average oxidation states of transition metals were determined by ICP-AES and iodometry, respectively [8]. SEM observations and specific surface area measurements by BET method were performed for several representative samples.

Electrochemical properties were examined with CR2032 type coin cells. The cell was comprised of a cathode and lithium metal anode separated by a polypropylene separator and glass fiber mat. The cathode consisted of 25 mg of $LiNi_{1/3}Co_{1/3}Mn_{1/3}O_2$ powders and 12 mg conducting binder pressed on a stainless screen. The electrolyte solution was 1 M $LiPF_6$/EC and DMC. The EC and DMC were mixed in a 1:2 volume ratio. The cell was charged and discharged in the voltage range of 2.5–4.3 V at a current density of 0.4 mA cm^{-2} at 23 °C.

3. Results and discussion

3.1. Calcination temperature dependence of stoichiometric $LiNi_{1/3}Co_{1/3}Mn_{1/3}O_2$

3.1.1. Chemical composition and oxidation state

The chemical compositions analyzed by ICP-AES and the average formal valences of transition metals (TM) calculated from the chemical compositions are shown in Table 1. For all the samples, the Ni/Co/Mn molar ratios are almost identical, and the Li/transition metals molar ratios distribute in the narrow range from 1.01 to 1.04. The Li compositions are slightly excess from the stoichiometric ones. Both the formal valences of transition metals calculated from the observed chemical compositions, V_c, and the average valences of transition metals from iodometry, V_o, are slightly larger than 3.0.

Fig. 2 shows the dependence of the average valence for transition metals on the calcination temperature. The ordinate shows the difference between the observed and calculated valence; $\Delta = V_o - V_c$. As the calcination temperature is raised up, the Δ increases. Cho et al. studied the oxidation state

Table 1
Chemical compositions of $LiNi_{1/3}Co_{1/3}Mn_{1/3}O_2$ prepared at various temperatures from 800 to 1100 °C

Temperature (°C)	Chemical formula	Formal valence	Valence from iodometry
800	$Li_{1.04}Ni_{0.34}Co_{0.33}Mn_{0.33}O_2$	3.04	3.05
850	$Li_{1.04}Ni_{0.34}Co_{0.33}Mn_{0.33}O_2$	3.04	3.06
900	$Li_{1.04}Ni_{0.34}Co_{0.33}Mn_{0.33}O_2$	3.04	3.06
950	$Li_{1.04}Ni_{0.34}Co_{0.33}Mn_{0.33}O_2$	3.04	3.06
1000	$Li_{1.02}Ni_{0.34}Co_{0.33}Mn_{0.33}O_2$	3.02	3.06
1050	$Li_{1.04}Ni_{0.34}Co_{0.33}Mn_{0.33}O_2$	3.04	3.09
1100	$Li_{1.01}Ni_{0.34}Co_{0.33}Mn_{0.33}O_2$	3.01	3.08

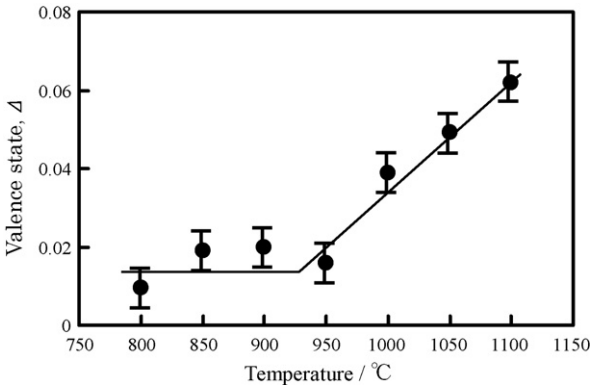

Fig. 2. The calcination temperature dependence of the average oxidation state of transition metals for $LiNi_{1/3}Co_{1/3}Mn_{1/3}O_2$. The ordinate shows the difference, $\Delta = V_o - V_c$, between the valence determined by iodometry, V_o, and the valence calculated from chemical compositions, V_c.

of each transition metal species for $LiNi_{1/3}Co_{1/3}Mn_{1/3}O_2$ using XPS [9]. Their results indicate that the high calcination temperature leads to the change in the oxidation states from those of Ni^{2+}, Co^{3+} and Mn^{4+} reported for the sample calcined at lower temperature by the XANES measurements [10]. However, the specific origins of the change in the oxidation state have not been clarified in their study. If $LiNi_{1/3}Co_{1/3}Mn_{1/3}O_2$ adopts the single phase with the layered rock-salt structure in all the temperature ranges, the oxidation state should be rather reduced with increasing the temperature. Because the dissociation pressure of oxygen from the solid oxide in the heterogeneous reaction: $LiNi_{1/3}Co_{1/3}Mn_{1/3}O_2 \leftrightarrow LiNi_{1/3}Co_{1/3}Mn_{1/3}O_{2-\delta} + \delta/2O_2$ should depend only on the temperature. However, the observed dependence of the average valence of transition metals on the calcination temperature is opposite. It is suggested that the $LiNi_{1/3}Co_{1/3}Mn_{1/3}O_2$ calcined at higher temperature forms the small amount of impurity phases containing transition metals with higher valence.

3.1.2. Powder X-ray diffraction

The powder XRD patterns of $LiNi_{1/3}Co_{1/3}Mn_{1/3}O_2$ samples calcined at various temperatures are shown in Fig. 3. All the diffraction patterns can be indexed assuming a layered rock-salt structure and do not show any intense peaks of the second phase. The details of the XRD patterns are shown in Fig. 4 as logarithmic plots of intensity. A quite weak extra diffraction peak emerges at around $2\theta = 31^\circ$ in the patterns of the samples calcined at 1100 and 1150 °C. The intensity of the extra peak increases with raising the calcination temperature. The *d*-value of the extra peak is 2.88 Å, which is about the twice of the *d* (11.0) = 1.43 Å of α-$NaFeO_2$-type structure. This value also corresponds to the 220 lattice spacing of cubic spinel with the lattice parameter of $a = 8.15$ Å. However, most peaks of the spinel and the layered structure overlap, and the intensity of the isolated 220 reflection of a spinel structure is quite weak. The fraction of the spinel structure was evaluated from the intensity ratio of the 220 peak for a spinel structure and the 00.6 peak for a layered structure. The peak

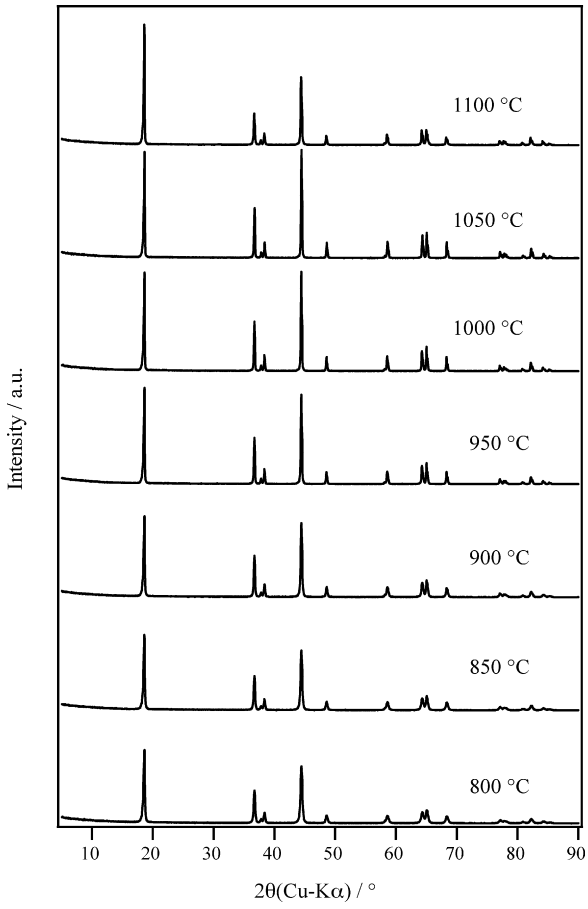

Fig. 3. X-ray diffraction patterns of $LiNi_{1/3}Co_{1/3}Mn_{1/3}O_2$ prepared at different temperatures from 800 to 1100 °C.

intensity ratio, *I*(220)/*I*(00.6), calculated using Rietan-2000 program for the 1:1 mixture in weight of $LiNi_{1/3}Co_{1/3}Mn_{1/3}O_2$ with α-$NaFeO_2$ type structure and $Li(Ni_{1/3}Co_{1/3}Mn_{1/3})_2O_4$ with spinel-type structure is 1.67. For the sample calcined at 1150 °C, the observed intensity ratio, *I*(220)/*I*(00.6), is 0.022. The fraction of spinel structure was roughly evaluated to be 1.3 wt%.

The lattice parameters were obtained by a least squares method using diffraction peaks in the 2θ range from 55° to 70°. They are plotted in Fig. 5 as a function of the calcination temperature. Lattice parameters and unit cell volumes increase monotonically with increasing the calcination temperature. However, the *c*/*a* ratios are almost constant. The observed variation of lattice parameters with the temperature is quite different from those in the following two systems: (1) the system with the cation exchange between Li and transition metal layers and (2) the system with the electrochemical de-intercalation of lithium-ion. In the former case, the increasing the Ni fraction in the Li 3a-sites causes the decrease of the *c*/*a* ratio as reported for $LiNi_{0.8}Co_{0.2}O_2$ [11]. In the latter case such as Li/$LiNi_{1/3}Co_{1/3}Mn_{1/3}O_2$ cell, the lattice parameter, *a* decreases and *c* increases with the increase of de-intercalated Li^+ [12]. In both cases, lattice strains are anisotropic, while the *c*/*a* ratios of the present samples are almost constant.

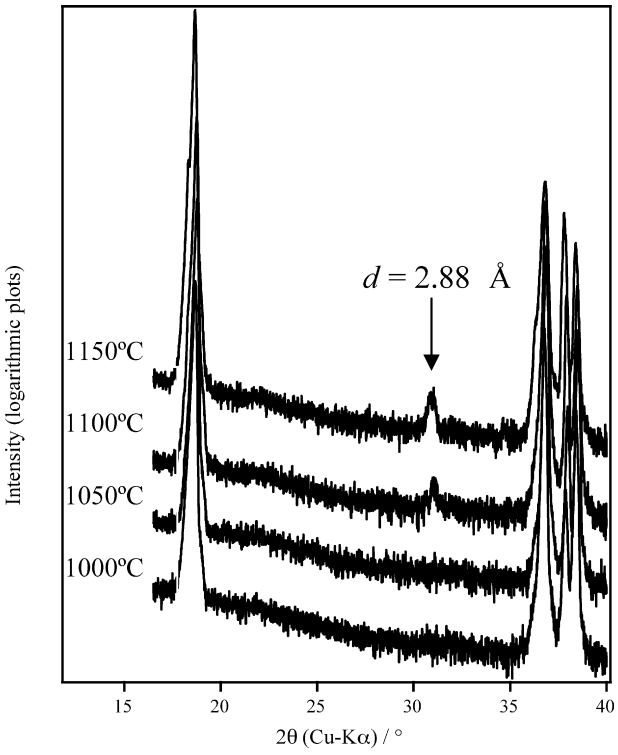

Fig. 4. Enlarged X-ray diffraction patterns (logarithmic plots) of $LiNi_{1/3}Co_{1/3}Mn_{1/3}O_2$ prepared at 1000, 1050, 1100 and 1150 °C. The arrow indicates the extra peak corresponding to the 220 reflection of a cubic spinel structure.

A series of Rietveld analysis was performed to monitor the structural change with calcination temperature. The results are summarized in Table 2. Calculations were made by assuming the space group symmetry of $R\bar{3}m$. Ideally, Ni, Co and Mn atoms are randomly placed on 3b-sites and Li atoms occupy 3a-sites. This model does not reproduce the observed profiles. The site exchange of Li atoms with Ni atoms was assumed. The refinements gave good agreement factors of R_{wp} in the range from 8.55 to 11.3% and the scale factors, s, in the range from 1.20 to 1.46 for the samples calcined at 850–1000 °C. The scale factor smaller than 1.5 indicates the goodness of fitting. However, the refinement for the sample calcined at 1050 °C yielded larger R_{wp} and s factors. The preferential orientation and/or the sintering of the small particles due to the high temperature calcination may be the origin. The refined values of the fraction of Ni^{2+} ions in the lithium layer (3a-site) are in the range from 2.8 to 4.9% and they are apt to increase with raising the calcination temperature.

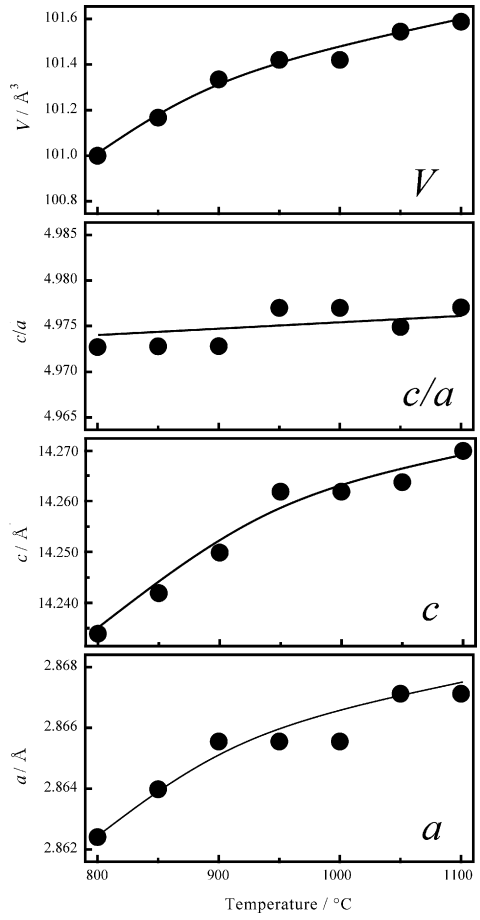

Fig. 5. The dependence of lattice parameters and unit cell volumes of $LiNi_{1/3}Co_{1/3}Mn_{1/3}O_2$ on the calcination temperature.

3.1.3. Electron diffraction and TEM study

Fig. 6 shows a TEM image and an [00.1] zone electron diffraction pattern (EDP) of a particle in the sample calcined at 1000 °C, respectively. The [00.1] zone electron diffraction pattern in Fig. 6 shows two kinds of extra spots: (1) those indicating $[\sqrt{3} \times \sqrt{3}]R30°$ ordering in the basal plane as marked by arrows in the figures, and (2) those marked by an asterisk, indicating 2×2 ordering. The number of particles showing the extra spots of the 2×2 ordering is less than 10% among all observed particles. The extra spots of the 2×2 ordering are much stronger than those of the $\sqrt{3} \times \sqrt{3}$ ordering. The extra spots of the 2×2 ordering could not be observed for the sample calcined at 900 °C at all, but most of the particles in the sample calcined at 1100 °C show the extra spots.

Table 2
The results of the Rietveld analyses for $LiNi_{1/3}Co_{1/3}Mn_{1/3}O_2$

Calcination temperature (°C)	Fraction of Ni in the Li 3a-sites (%)	Lattice parameters		Reliability factors and a scale factor			
		a (Å)	c (Å)	R_{wp} (%)	R_p (%)	R_e (%)	s
850	2.79	2.862	14.23	10.5	6.87	8.69	1.20
900	3.83	2.864	14.24	8.61	7.27	8.40	1.28
950	3.29	2.866	14.25	8.55	7.50	8.34	1.36
1000	3.50	2.866	14.26	11.3	8.49	8.83	1.46
1050	4.88	2.867	14.26	13.9	13.4	8.42	2.10

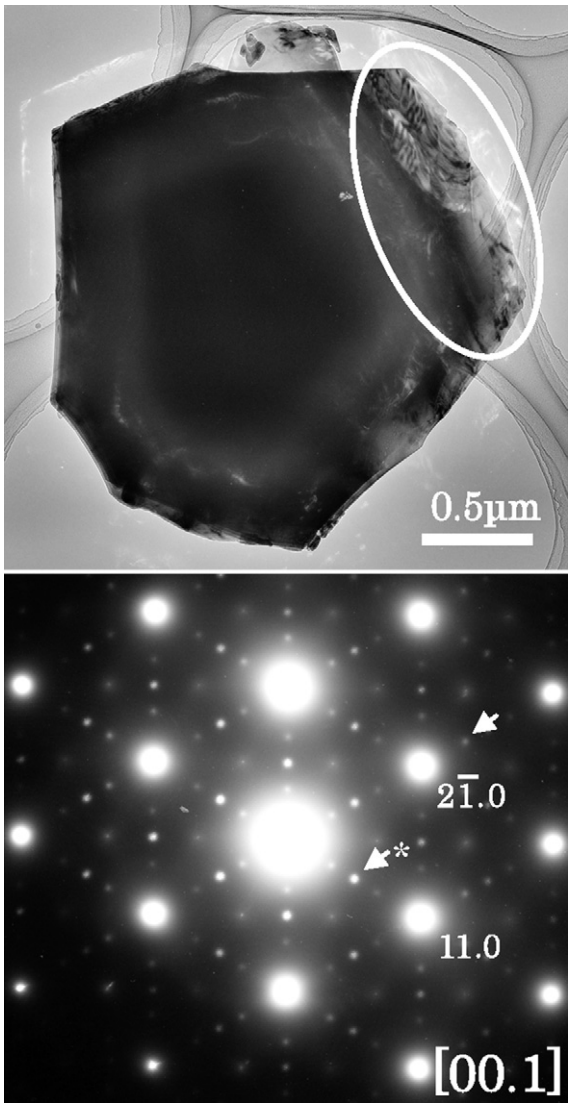

Fig. 6. A low magnification TEM image and an electron diffraction pattern of the $LiNi_{1/3}Co_{1/3}Mn_{1/3}O_2$ calcined at 1000 °C for 12 h in air stream. The diffraction spots have been indexed based on the hexagonal system. Extra spots indicating a 2×2 superlattice are seen as indicated by an arrow with the asterisk. The arrow without the asterisk indicates very weak extra spots of a $\sqrt{3} \times \sqrt{3}$ superlattice.

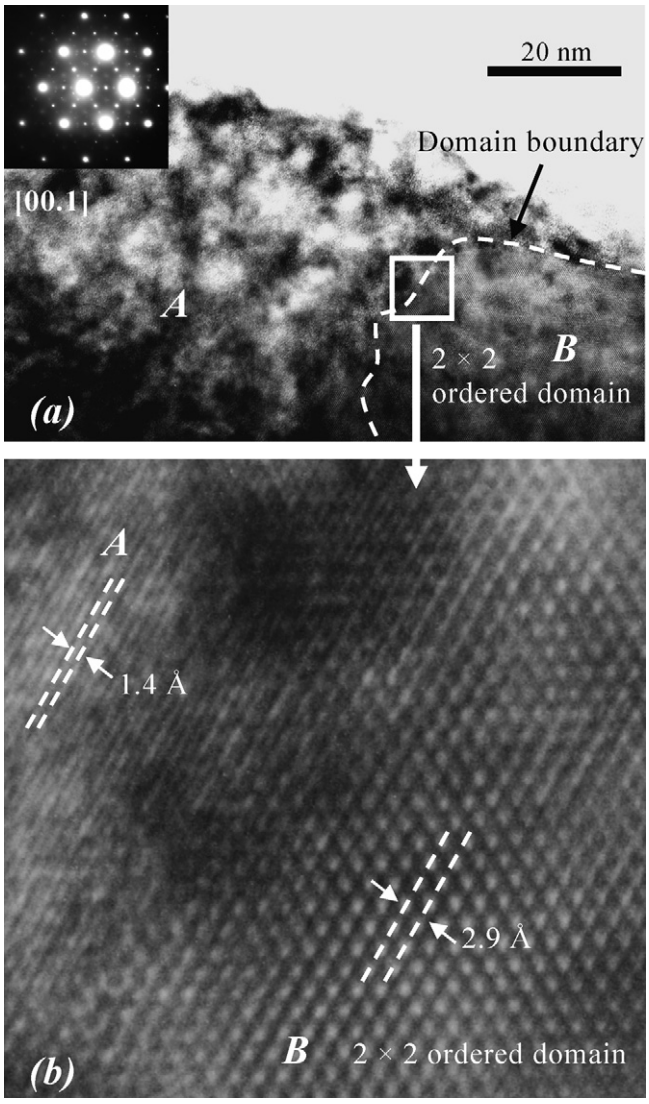

Fig. 7. A lattice image with the $[00.1]_{hexa.}$ incidence for $LiNi_{1/3}Co_{1/3}Mn_{1/3}O_2$ calcined at 1000 °C.

The lattice image viewed along the [00.1] direction of rhombo-hexagonal system and the corresponding EDP are shown in Fig. 7(a). The particle in Fig. 7(a) consists of two types of domains. Fig. 7(b) shows the enlarged image of the region marked by the square in Fig. 7(a). In the region A, the image shows the (11.0) lattice fringe with the *d*-spacing of 1.4 Å. However in the region B, it shows the lattice fringe with the spacing of 2.9 Å, which is twice the (11.0) lattice spacing, indicating the 2×2 ordering. Both type domains are coherently intergrown in one particle. The average domain size of the 2×2 ordered domain is about 30 nm.

The one of possible origins for the 2×2 ordering is the coherent precipitation of spinel-like phases in the matrix of α-$NaFeO_2$ type structure. In the planar triangular lattice, the ordering of the metal atoms and their vacancies in a ratio of 3:1 leads to the 2×2 ordering. In the spinel-type structure, we can see such an ordering. The appearance of the clear 220 peak of the spinel-like phase in the XRD patterns for the samples calcined at 1100 and 1150 °C suggests that the small embrios of the spinel-like structure are embedded even in the sample annealed at 1000 °C. The formation of the spinel-like phase leads to the valence state of transition metals higher than 3.0 as observed for the present samples.

Another possible origin of the 2×2 ordering might be the occupation of the Li atoms in the tetrahedral sites and their ordering. However, there are no reports on such an ordering. Also the 2×2 ordering of Li atoms and their vacancies as reported for Li_xNiO_2 with $0.5 < x < 0.7$ [13] is not plausible, because the present samples show the nearly equal composition of Li and transition metal atoms.

3.1.4. Morphology

Fig. 8 shows SEM images and BET-specific surface areas of $LiNi_{1/3}Co_{1/3}Mn_{1/3}O_2$ samples. The sample calcined at 800 °C

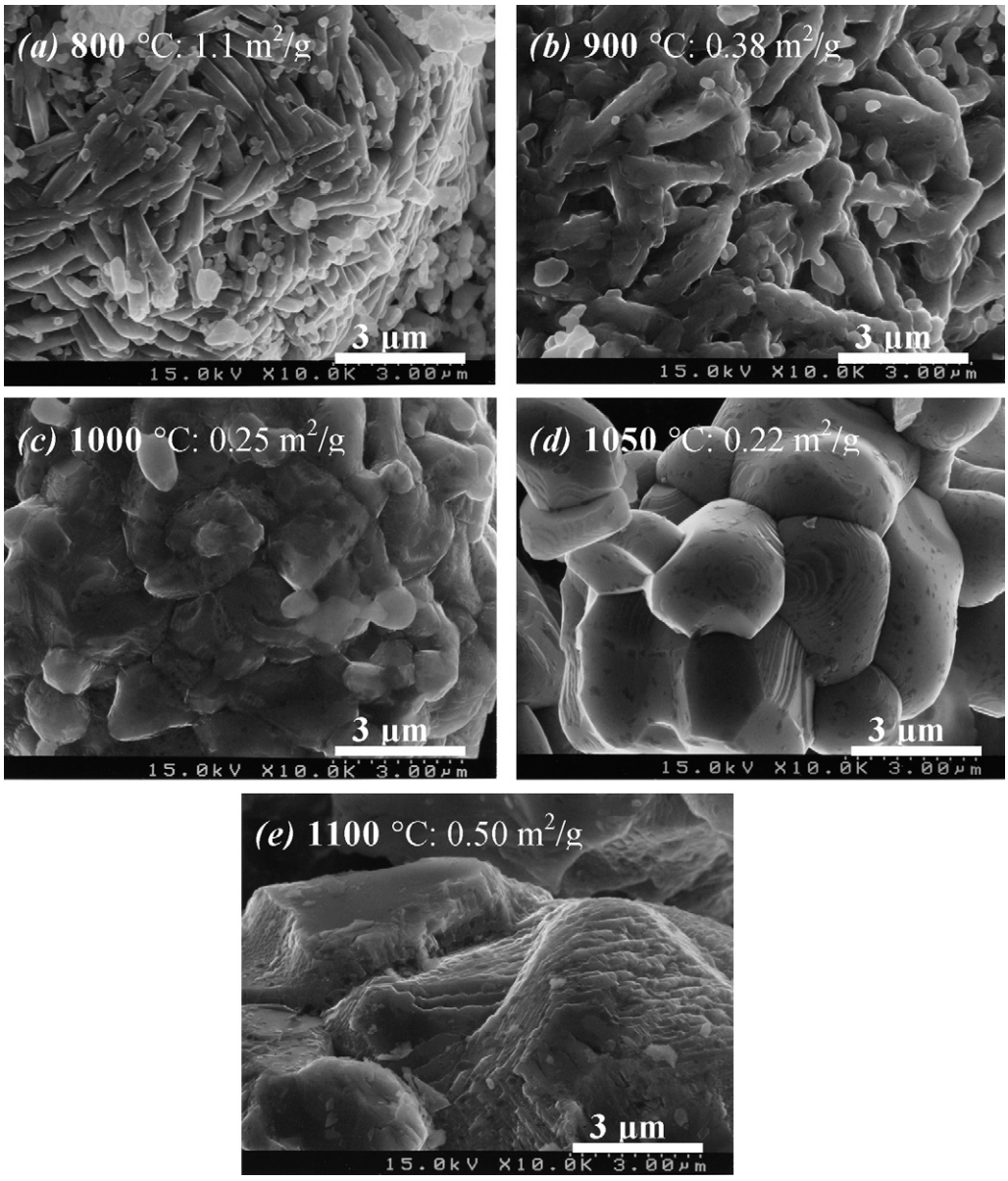

Fig. 8. SEM images and BET specific surface areas of $LiNi_{1/3}Co_{1/3}Mn_{1/3}O_2$ samples prepared at various temperatures. (a) 1.1 $m^2\,g^{-1}$ calcined at 800 °C, (b) 0.38 $m^2\,g^{-1}$ calcined at 900 °C, (c) 0.25 $m^2\,g^{-1}$ calcined at 1000 °C, (d) 0.22 $m^2\,g^{-1}$ calcined at 1050 °C and (e) 0.50 $m^2\,g^{-1}$ calcined at 1100 °C.

reveal the plate-like primary particles with hexagonal habit. With increasing the temperature, primary particles tend to sinter into coarse particles and the plate-like primary particles with hexagonal habit cannot be seen. For the sample calcined at 800 °C, BET specific surface area is 1.1 $m^2\,g^{-1}$. With increasing the calcination temperature from 900 to 1050 °C, BET specific surface areas are quite low in the range of 0.2–0.4 $m^2\,g^{-1}$ and tend to decrease. While the sample calcined at 1050 °C reveals the quite smooth surface, some surface roughening is indicated from the SEM image for the sample calcined at 1100 °C. Some fine particles seem to deposit on the surface. BET-specific surface area for the samples calcined at 1100 °C is larger than that for the samples at 1050 °C, in spite of the lower surface area with the higher calcination temperature between 900 and 1050 °C. The increase in the roughness of the particle surface and specific surface area for the sample calcined at 1100 °C may originate from the coprecipitation of the spinel-like phase.

3.1.5. Electrochemical properties

Fig. 9(a) shows the charge and discharge curves for $LiNi_{1/3}Co_{1/3}Mn_{1/3}O_2$ samples calcined at different temperatures. They were measured at a current density of 0.4 mA cm^{-2} between 2.5 and 4.3 V for the first cycle. All the profiles show the single plateaus with an average potential near 3.8 V. The profiles for the samples calcined at 800 and 900 °C give the rechargeable capacities of ca. 155 mAh g^{-1}. The capacities are somewhat smaller than those in the recent literatures about 165 mAh g^{-1} [1–4]. The difference may be originated from the difference in the powder characteristic of samples like grain size and surface

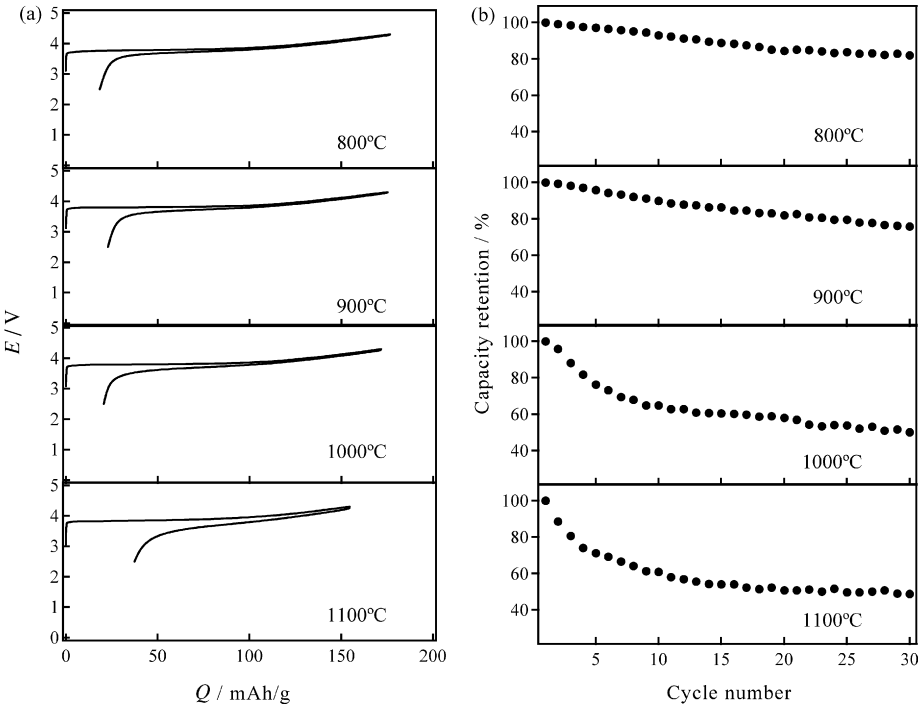

Fig. 9. (a) Charge and discharge curves and (b) cycle performances of Li/$LiNi_{1/3}Co_{1/3}Mn_{1/3}O_2$ cells operated at 0.4 mA cm^{-2} in the voltage range of 2.5–4.3 V at 23 °C. $LiNi_{1/3}Co_{1/3}Mn_{1/3}O_2$ samples were prepared at different temperatures in the range from 800 to 1100 °C.

area. The significant capacity fading and polarization were observed for the samples calcined at higher temperatures. The degraded profile for the sample calcined at 1100 °C shows no noticeable plateaus at around 3 V indicative of the formation of the spinel-like phase, as is observed for the spinel phase converted from the monoclinic or orthorhombic phase $LiMnO_2$ [14,15]. Fig. 9(b) also indicates that the cycle performance of $LiNi_{1/3}Co_{1/3}Mn_{1/3}O_2$ samples deteriorated with increasing the calcination temperature. The samples calcined at higher temperatures also cycle with the much more loss of rechargeable capacity.

The decline of the electrochemical properties for samples calcined at higher temperatures correlates with the change in the local structure. The deterioration is significant for the samples of which EDPs show the 2×2 type extra spots indicative of the coherent formation of the spinel-like domain. The delivered capacity decreases with the increase of the oxidation states of transition metals as confirmed by iodometry. However, the effect of the 2×2 ordering on the cycle performance is not fully understood at present stage.

The similar 2×2 type extra spots in the ED patterns have been reported for the degraded $LiCoO_2$ samples after long term cycling, although the no change was observed in their XRD patterns [16]. It was also indicated that such extra spots can be responsible for the formation of the cation vacancy in the heavily cycled $LiCoO_2$ sample.

The lower capacity for the samples calcined at higher temperature is caused not only by the change in the local structure, but also by the increase of the particle size. The low surface area and long diffusion distance inside the primary particles cause the capacities to decrease [17].

3.2. Li composition dependence on structures and properties for $Li_xNi_{1/3}Co_{1/3}Mn_{1/3}O_2$

As described in the previous section, in the case of stoichiometric $LiNi_{1/3}Co_{1/3}Mn_{1/3}O_2$ samples calcined at high temperatures, vacancies are formed in the transition metal layers with the spinel-like ordering and the electrochemical properties are deteriorated. The optimum calcination temperature to obtain the nearly stoichiometric powder samples with good electrochemical properties and the high packing density is 900 °C. The effects of the Li composition on the crystal structure and electrochemical properties have been studied for the samples with the composition of $Li_xNi_{1/3}Co_{1/3}Mn_{1/3}O_2$ ($0.742 \leq x \leq 1.12$) calcined at 900 °C for 12 h in air. The other layered rock salt oxides with deficient Li compositions, $Li_{0.5}MO_2$ (M: Ni, Co and Mn), obtained by chemically extracting Li were confirmed to transform to the spinel-like phases by heating [18]. The formation of the spinel-like second phase in $Li_xNi_{1/3}Co_{1/3}Mn_{1/3}O_2$ ($x < 1.0$) is strongly suggested.

3.2.1. Powder X-ray diffraction

The powder XRD patterns of $Li_xNi_{1/3}Co_{1/3}Mn_{1/3}O_2$ samples are shown in Fig. 10 on semi-log plots. The Li compositions, x, were 0.742, 0.884, 0.999, 1.08 and 1.12, respectively. All the peaks can be indexed assuming a layered rock-salt structure. However, Li deficient samples show a peak of the second phase at around $2\theta = 31°$ ($d = 2.87$ Å) and it grows up with increasing Li-deficiency. The d-value corresponds to the (220) lattice spacing of cubic spinel phase, similarly to those of the stoichiometric samples calcined at high temperatures. Fig. 11 shows the lattice

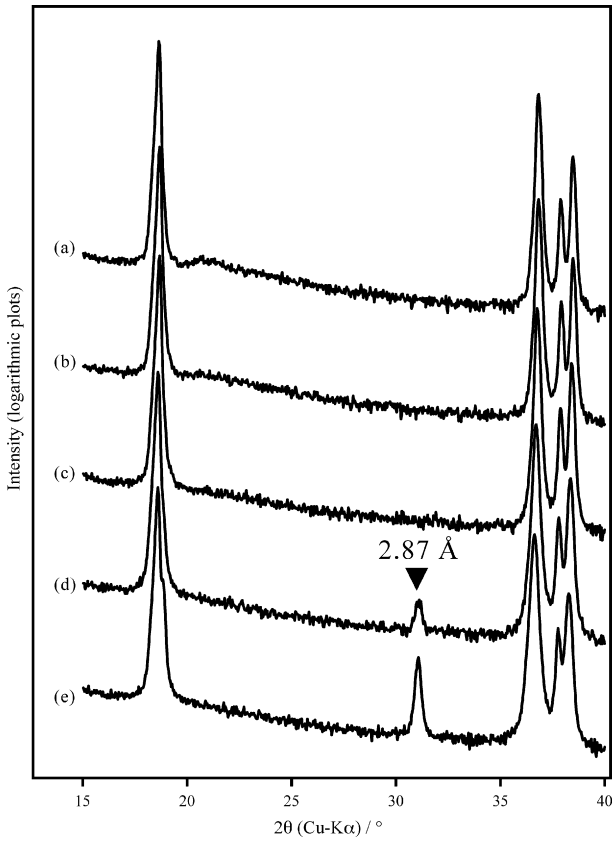

Fig. 10. X-ray diffraction patterns (logarithmic plots) of $Li_xNi_{1/3}Co_{1/3}Mn_{1/3}O_2$ calcined at 900 °C for 12 h in air stream. (a) $x = 1.12$, (b) $x = 1.08$, (c) $x = 0.999$, (d) $x = 0.884$ and (e) $x = 0.742$. The arrow and the asterisk indicate the 220 reflection of a cubic spinel structure.

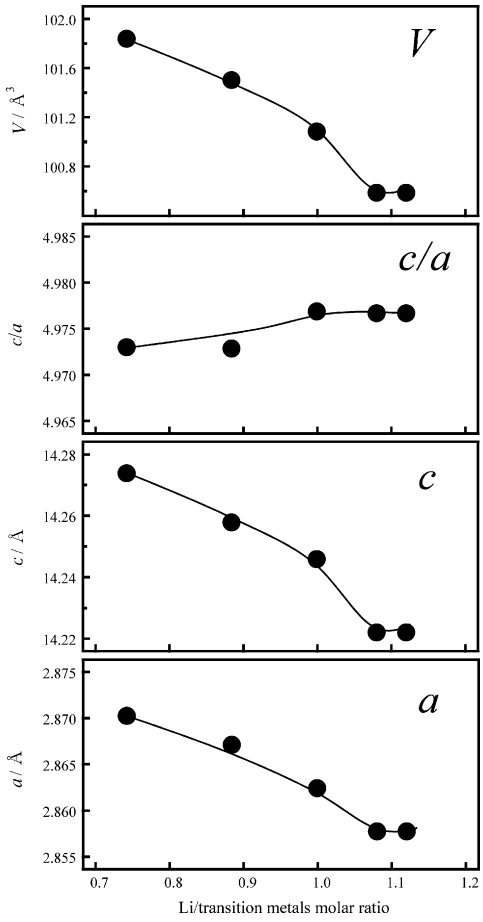

Fig. 11. The dependence of lattice parameters and the unit cell volume for $Li_xNi_{1/3}Co_{1/3}Mn_{1/3}O_2$ ($0.742 \leq x \leq 1.12$) on the Li composition.

parameters of $Li_xNi_{1/3}Co_{1/3}Mn_{1/3}O_2$ as a function of Li composition. The lattice parameters and the unit cell volumes increase with the Li deficiency in the range below $x = 1.08$, while the *c*/*a* ratios are almost constant. Their variations are similar to those of the stoichiometric $LiNi_{1/3}Co_{1/3}Mn_{1/3}O_2$ samples with increasing the calcination temperature. According to the above result, it is plausible that the stoichiometric $LiNi_{1/3}Co_{1/3}Mn_{1/3}O_2$ calcined at high temperatures decomposes to form the spinel-like phase with Li-rich phase, $Li(Li_xM_{1-x})O_2$ (M: transition metals) or Li_2CO_3. However, we cannot specify the detail of the Li-rich decomposition products at present stage.

3.2.2. Electrochemical properties

The effect of the Li composition on the electrochemical properties for $Li_xNi_{1/3}Co_{1/3}Mn_{1/3}O_2$ ($0.742 \leq x \leq 1.12$) has been investigated. Fig. 12(a) shows the charge and discharge curves for the first cycle measured in the same conditions as described in Section 3.1.5. All the profiles show single plateaus with an average potential near 3.8 V. The significant capacity fading and noticeable polarization were observed for the samples with the low Li-compositions. The sample with excess Li, $x = 1.12$ also shows the smaller capacity than those for the samples with $x = 0.999$ and 1.08. The smaller capacity for the sample with $x = 1.12$ may be responsible for the higher oxidation states of transition metals due to the charge compensation with the Li-excess composition, $[Li]_{3a}[(Ni_{1/3}Co_{1/3}Mn_{1/3})_{1-y}Li_y]_{3b}O_2$. As shown in Fig. 12(b), the cycle performance of $Li_xNi_{1/3}Co_{1/3}Mn_{1/3}O_2$ samples also degraded with increasing Li-deficiency. The degradation in the electrochemical properties for $Li_xNi_{1/3}Co_{1/3}Mn_{1/3}O_2$ with decreasing the Li composition is similar to that for nearly stoichiometric $LiNi_{1/3}Co_{1/3}Mn_{1/3}O_2$ with increasing the calcination temperature. These results may support the structural change in the stoichiometric $LiNi_{1/3}Co_{1/3}Mn_{1/3}O_2$ sample calcined at high temperature can be related to the decomposition of single phasic $LiNi_{1/3}Co_{1/3}Mn_{1/3}O_2$ to the spinel-like phase with the Li-deficient compositions and the residual phases.

On the other hand, the samples with the excess Li composition show better cycle performance with increasing the Li-composition. Such advantages of the Li-excess composition for $LiNi_{1/3}Co_{1/3}Mn_{1/3}O_2$ on electrochemical properties have been reported by several researchers [19–21]. However, the reason why the samples with excess Li show better properties than stoichiometric ones has not been clarified in their reports. The co-existence of spinel-like phase may be suppressed by the Li-excess composition, although the capacity decreases.

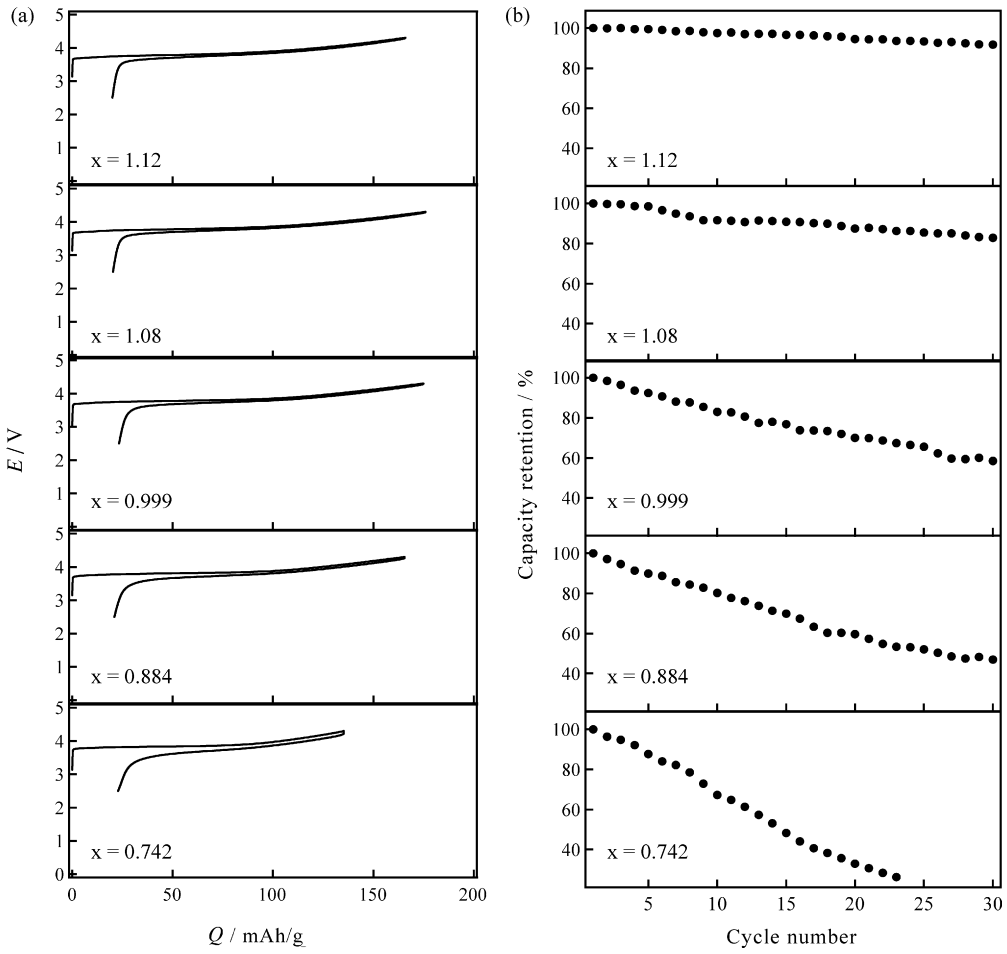

Fig. 12. (a) Charge and discharge curves and (b) cycle performances of Li/$Li_xNi_{1/3}Co_{1/3}Mn_{1/3}O_2$ ($0.742 \leq x \leq 1.12$) cells operated at 0.4 mA cm^{-2} in the voltage range of 2.5–4.3 V at 23 °C.

4. Conclusions

The structural and electrochemical properties of nearly stoichiometric $LiNi_{1/3}Co_{1/3}Mn_{1/3}O_2$ calcined at 800–1100 °C have been investigated. The specific surface area decreases and the particles tend to sinter with increasing the calcination temperature. No impurity phase was observed for the samples calcined at 800 and 900 °C and their electrochemical properties were good. For the samples calcined at 1000 °C and the higher temperatures, the local 2×2 ordered domain is coherently intergrown in one particle confirmed by ED and TEM observation. The high temperature calcination leads to the formation of vacancies in the transition metal layer and their spinel-like ordering. This is consistent with the increase of the unit cell parameters and the valence state of transition metals. The extra peak corresponding to the 220 reflection of spinel-like phase is absent in the XRD pattern for the sample calcined at 1000 °C, while the XRD patterns of the samples calcined at 1100 and 1150 °C show the clear extra peak. The small embrio of the spinel-like structure observed for the sample annealed at 1000 °C grows up with increasing the calcination temperature. The electrochemical properties of the samples tend to deteriorate when the calcination temperature is higher than 1000 °C. The decline of the electrochemical properties for samples calcined at higher temperatures correlates with the change in the local structure. The Li deficient $Li_xNi_{1/3}Co_{1/3}Mn_{1/3}O_2$ ($x \leq 0.89$) calcined at 900 °C contains the spinel-like second phase and shows the degraded electrochemical properties, similarly to the case of the stoichiometric $LiNi_{1/3}Co_{1/3}Mn_{1/3}O_2$ calcined at higher temperature. These results indicate that the change in the structural and electrochemical properties of nearly stoichiometric $LiNi_{1/3}Co_{1/3}Mn_{1/3}O_2$ calcined at high temperature is caused by the partial decomposition to the spinel-like phase with Li-deficient compositions and the Li-rich compounds. While densely packed particles prepared by high temperature calcination are desirable for the higher energy density of batteries, the calcination at the moderate temperature at around 900 °C is required in order to prepare stoichiometric $LiNi_{1/3}Co_{1/3}Mn_{1/3}O_2$ showing good electrochemical properties, and the slight Li-excess composition can be effective to avoid the formation of the spinel-like phase.

References

[1] T. Ohzuku, Y. Makimura, Chem. Lett. 7 (2001) 642.
[2] N. Yabuuchi, T. Ohzuku, J. Power Sources 119–121 (2003) 171.
[3] N. Yabuuchi, Y. Koyama, N. Nakayama, T. Ohzuku, J. Electrochem. Soc. 152 (2005) A1434.
[4] N. Yabuuchi, Y. Makimura, T. Ohzuku, J. Electrochem. Soc. 154 (2007) A314.

[5] S. Jouanneau, E. Bahmet, K.W. Eberman, L.J. Krause, J.R. Dahn, J. Electrochem. Soc. 151 (2004) A1789.
[6] E. Iwata, N. Suzuki, Japan, Patent, P2007-91573 (2007).
[7] T. Kamiyama, F. Izumi, H. Asano, H. Takagi, S. Uchida, E. Takayama-Muromachi, M. Matsuda, K. Yamada, Y. Endoh, Y. Hidaka, Physica C 172 (1990) 120.
[8] L.D. Dyyer, B.S. Borie Jr., G.P. Smith, J. Am. Chem. Soc. 76 (1954) 1499.
[9] T.H. Cho, S.M. Park, M. Yoshio, T. Hirai, Y. Hideshima, J. Power Sources 142 (2005) 306.
[10] H. Kobayashi, Y. Arachi, S. Emura, H. Kageyama, K. Tatsumi, T. Kamiyama, J. Power Sources 146 (2005) 640.
[11] R.K.B. Gover, R. Kanno, B.J. Mitchell, M. Yonemura, Y. Kawamoto, J. Electrochem. Soc. 147 (2000) 4045.
[12] D.-C. Li, T. Muta, L.-Q. Zhang, M. Yoshio, H. Noguchi, J. Power Sources 132 (2004) 150.
[13] J.P. Peres, F. Weill, C. Delmas, Solid State Ionics 116 (1999) 19.
[14] R.J. Gummow, D.C. Liles, M.M. Thackeray, Mater. Res. Bull. 28 (1993) 1249.
[15] M.R. Palacin, Y. Chabre, L. Dupont, M. Hervieu, P. Strobel, G. Masquwlier, M. Anne, G.G. Amatucci, J.M. Tarascon, J. Electrochem. Soc. 147 (2000) 845.
[16] H. Wang, Y.-I. Jang, B. Huang, D.R. Sadoway, Y.-M. Chiang, J. Electrochem. Soc. 146 (1999) 473.
[17] C.-C. Chang, J.Y. Kim, P.N. Kumta, J. Electrochem. Soc. 149 (2002) A1141.
[18] S. Choi, A. Manthiram, J. Electrochem. Soc. 149 (2002) A1157.
[19] S. Choi, A. Manthiram, Electrochem. Solid-State Lett. 7 (2004) A365.
[20] Y.M. Todorov, K. Numata, Electrochim. Acta 50 (2004) 495.
[21] J.-M. Kim, N. Kumagai, H.-T. Chung, Electrochem. Solid-State Lett. 9 (2006) A494.